High-Quality Cu–Al Nanocrystals for Enhanced CO_2 Electroreduction

Guanbo Wang[a,1], Hao Zhang[b,1], Jiahao Yang[a], Zeyi Lu[a], Wenqiong Li[a], Yanmei Tang[a], Yun He[a], Xiaoguang Liang[a,c,d,*], Xingyuan San[b,*], and Vellaisamy A. L. Roy[c,*]

[a]College of Physics and Technology, Guangxi Normal University & University Engineering Research Center of Advanced Functional Materials and Intelligent Sensing, Guilin, 541004, P. R. China

[b]Hebei Key Laboratory of Optic-electronic Information and Materials, The College of Physics Science and Technology, Hebei University, Baoding, 071002, China

[c]School of Science and Technology, Hong Kong Metropolitan University, Ho Man Tin, Hong Kong, P. R. China

[d]Guangxi Key Laboratory of Low Carbon Energy Materials, School of Chemical and Pharmaceutical Sciences, Guangxi Normal University, Guilin, 541004, P. R. China

*Corresponding authors: Xiaoguang Liang (lxg8521@gxnu.edu.cn), Xingyuan San (xysan@hbu.edu.cn), and Vellaisamy A. L. Roy (vroy@hkmu.edu.hk)

[1]These authors contributed equally to this work.

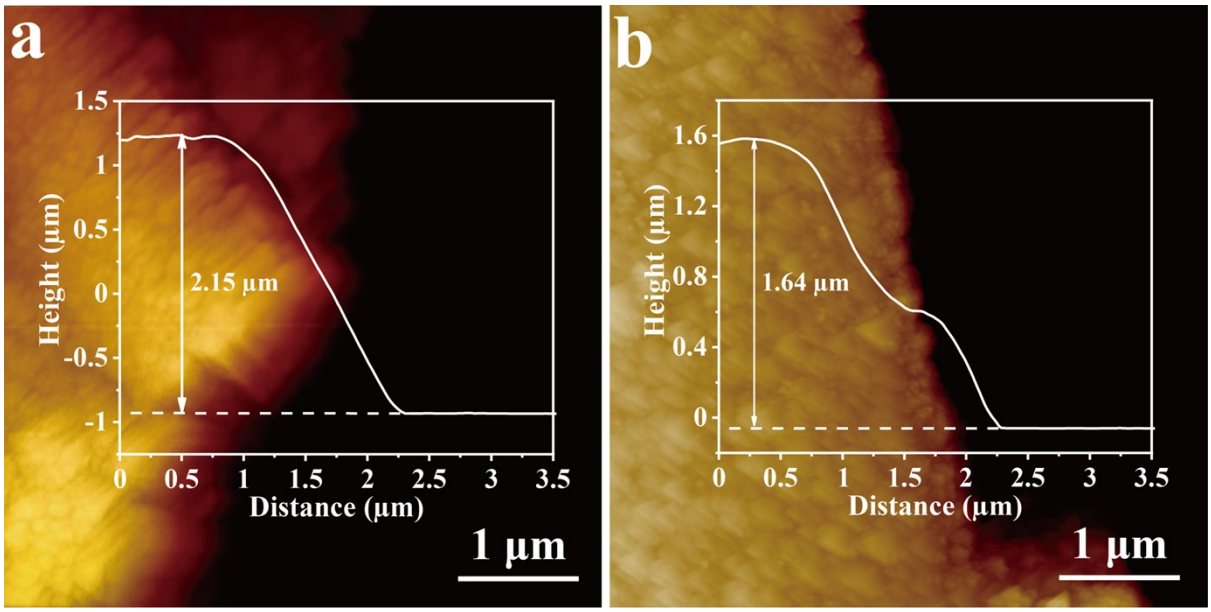

Figure S1. AFM images of (a) Cu and (b) Al thin films on Si wafer prepared by magnetron sputtering with the same deposition conditions as on carbon papers. The insets are the corresponding height profiles.

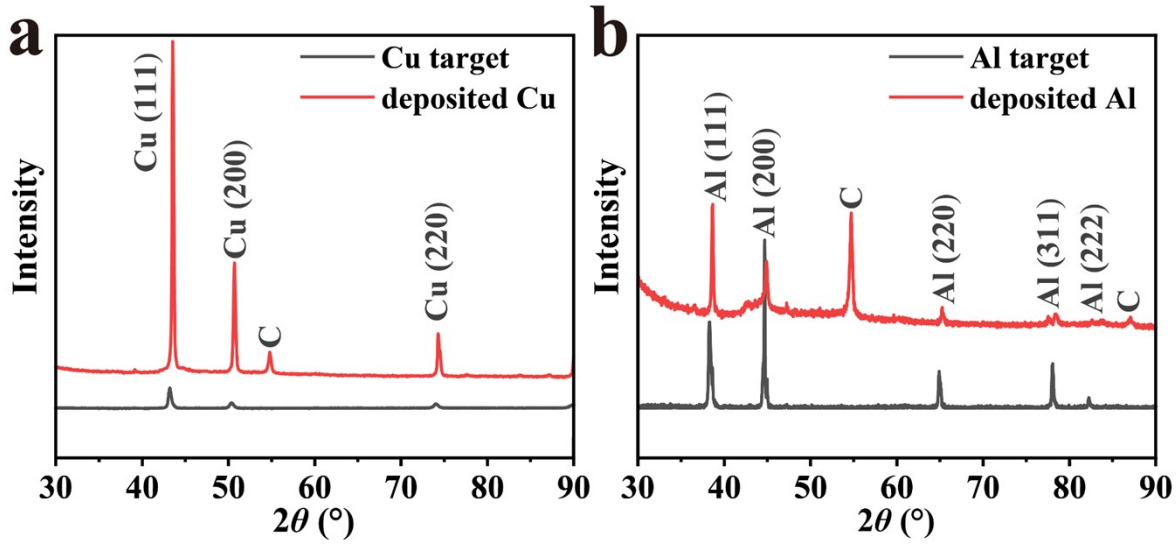

Figure S2. XRD patterns of (a) Cu and (b) Al targets and the deposited corresponding metals on carbon papers by magnetron sputtering.

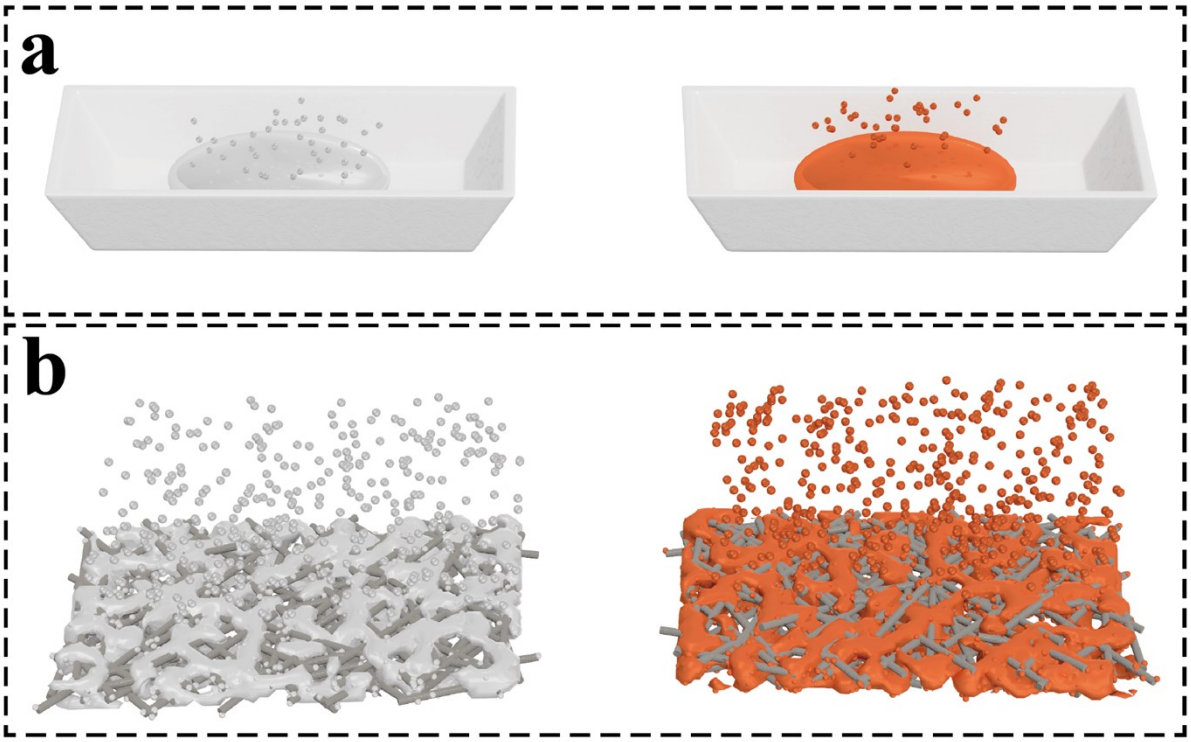

Figure S3. Schematic illustration for thermally excited atoms from (a) Cu and Al droplets formed via powder precursors and (b) Cu- and Al-covered carbon papers, respectively. Gray and brown represent Al and Cu, respectively.

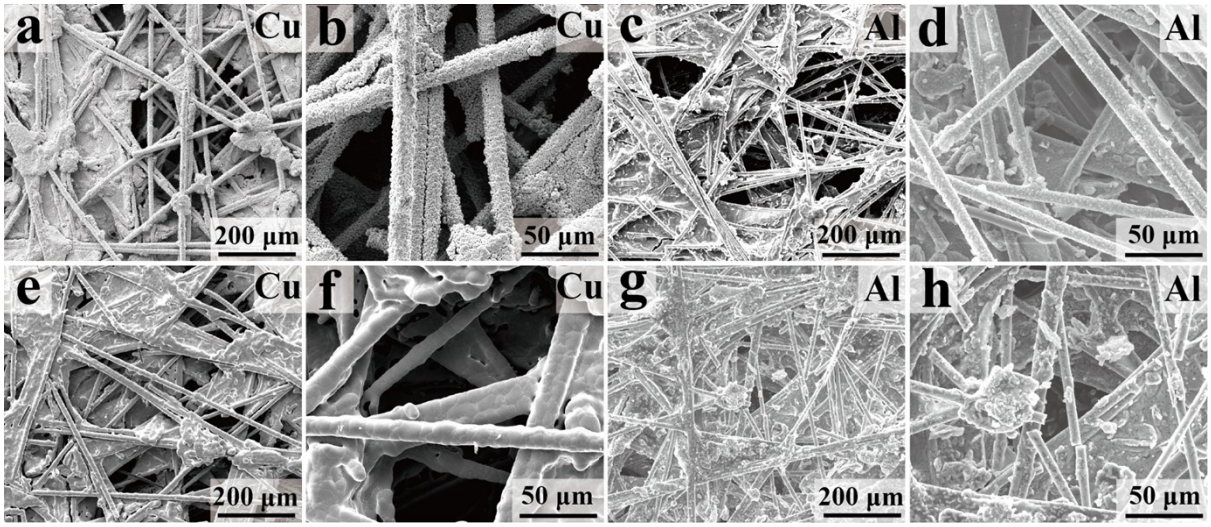

Figure S4. SEM images with different magnifications of the deposited Cu and Al on carbon papers (a–d) before and (e–f) after the CVD process.

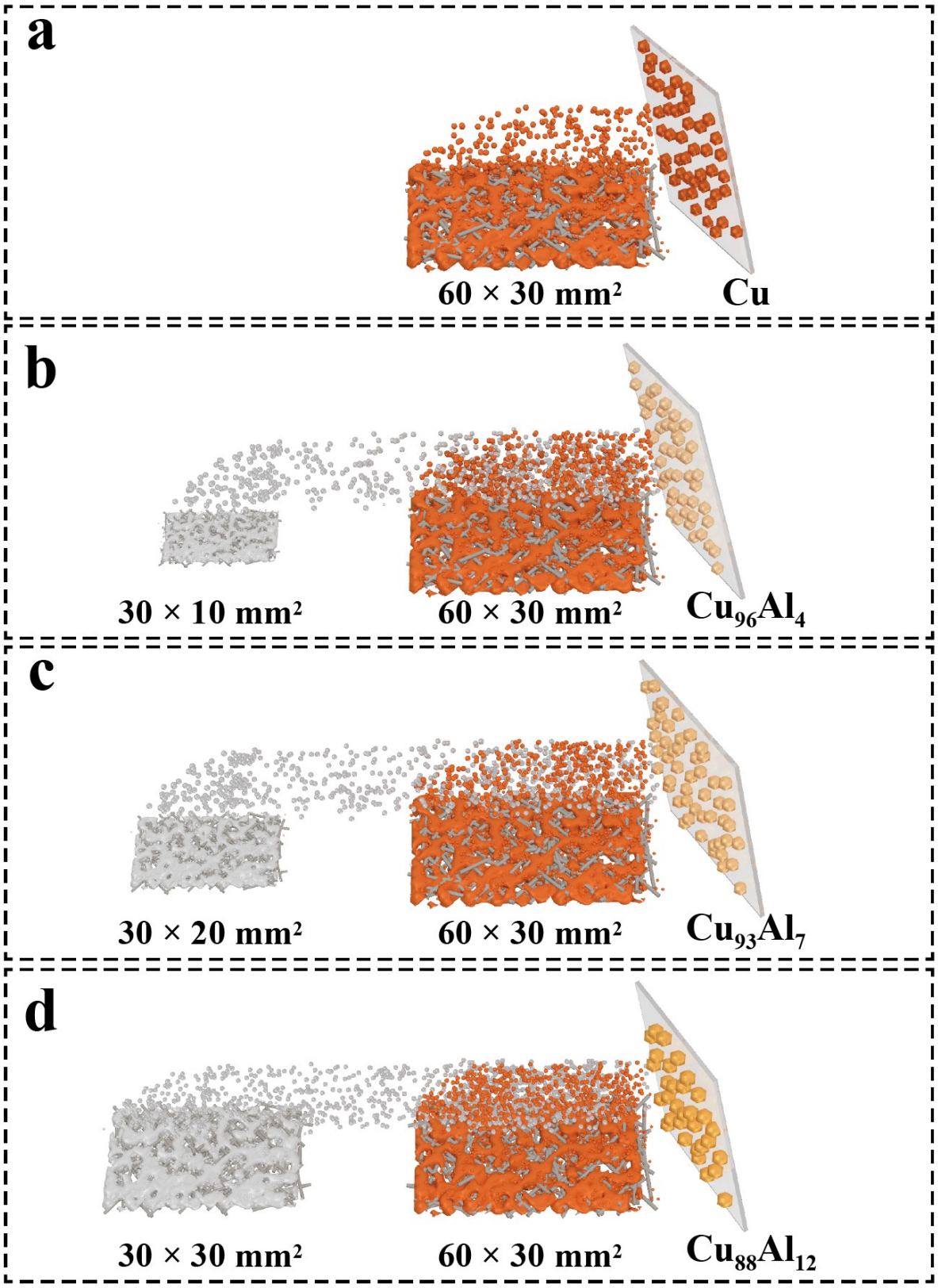

Figure S5. Schematic illustration for preparing (a) Cu, (b) $Cu_{96}Al_4$, (c) $Cu_{93}Al_7$, and (d) $Cu_{88}Al_{12}$ nanocrystals using Cu- and Al-deposited carbon paper with different sizes. Gray and brown represent Al and Cu, respectively.

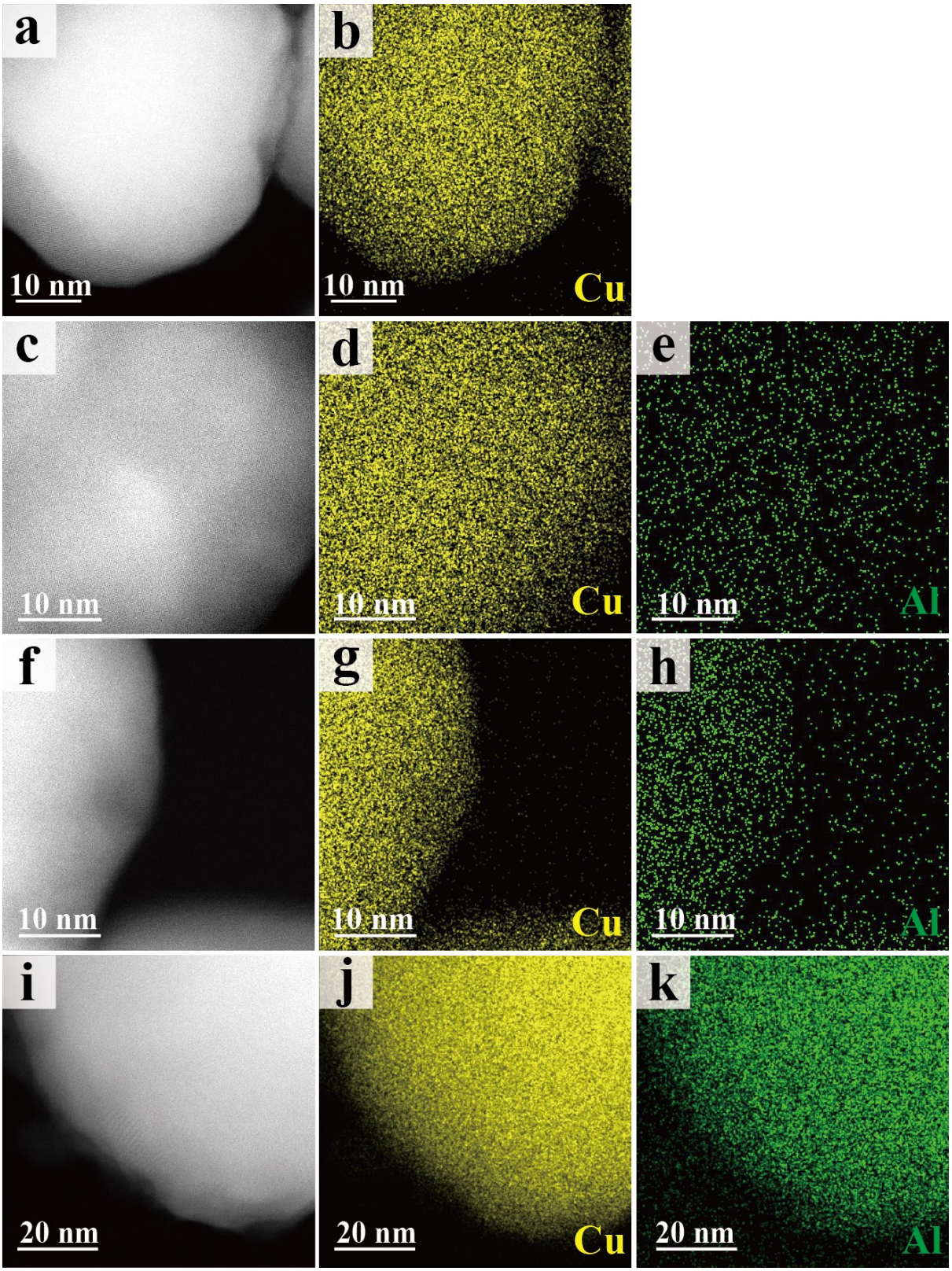

Figure S6. HAADF-STEM images and the corresponding EDS mappings of (a, b) Cu, (c–e) $Cu_{96}Al_4$, (f–h) $Cu_{93}Al_7$, and (i–k) $Cu_{88}Al_{12}$ single crystals.

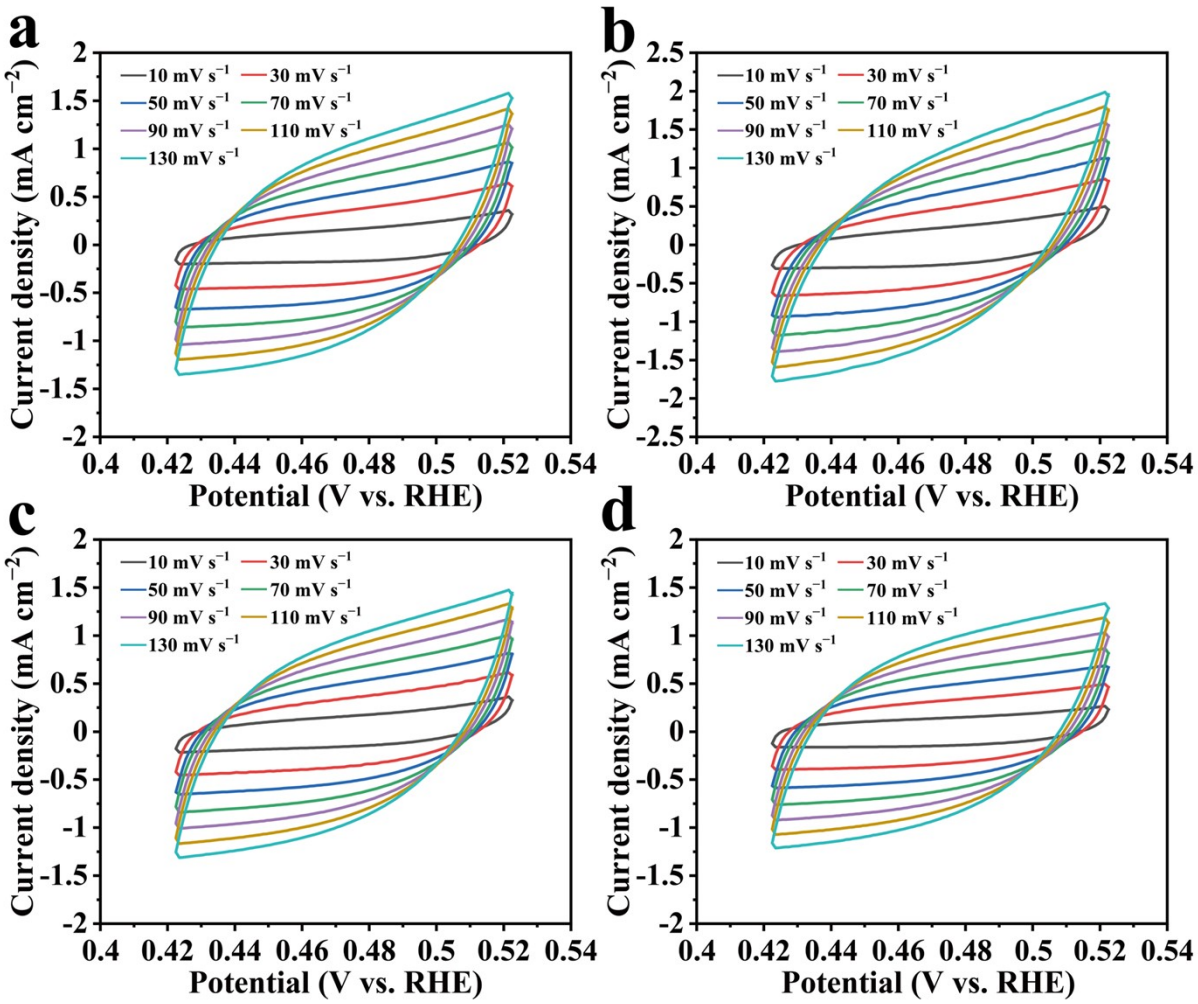

Figure S7. CV curves of (a) Cu, (b) $Cu_{96}Al_4$, (c) $Cu_{93}Al_7$, and (d) $Cu_{88}Al_{12}$ nanocrystals tested in the region from 0.42 to 0.52 V vs. RHE at scan rates from 10 to 130 mV s^{-1}.

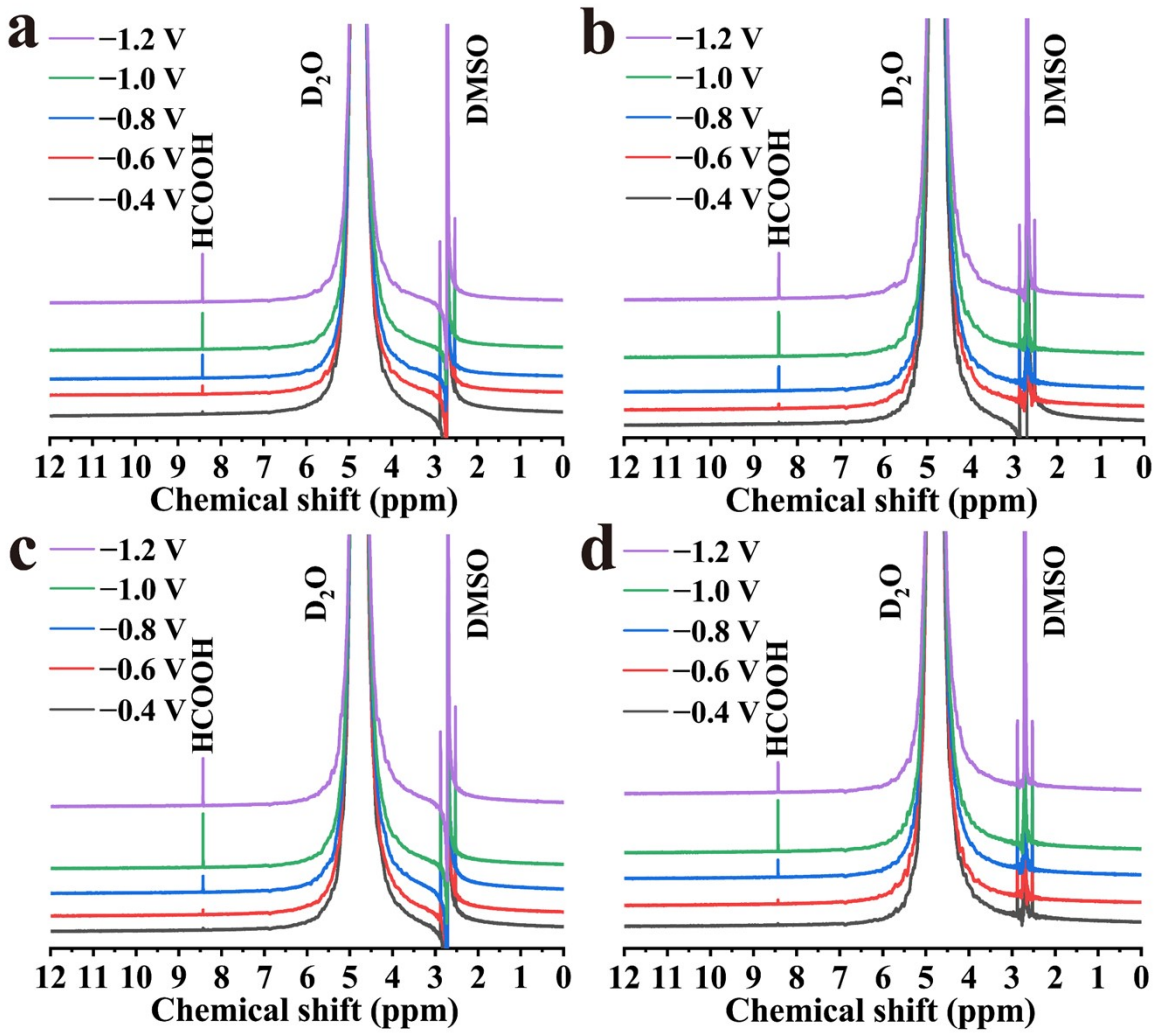

Figure S8. ^{1}H NMR spectra of the CO_2RR liquid products of (a) Cu, (b) $Cu_{96}Al_4$, (c) $Cu_{93}Al_7$, and (d) $Cu_{88}Al_{12}$ nanocrystals. The liquid samples were obtained after the catalytic reaction for 2 h at voltages of −0.4, –0.6, –0.8, –1, and −1.2 V vs. RHE, respectively.

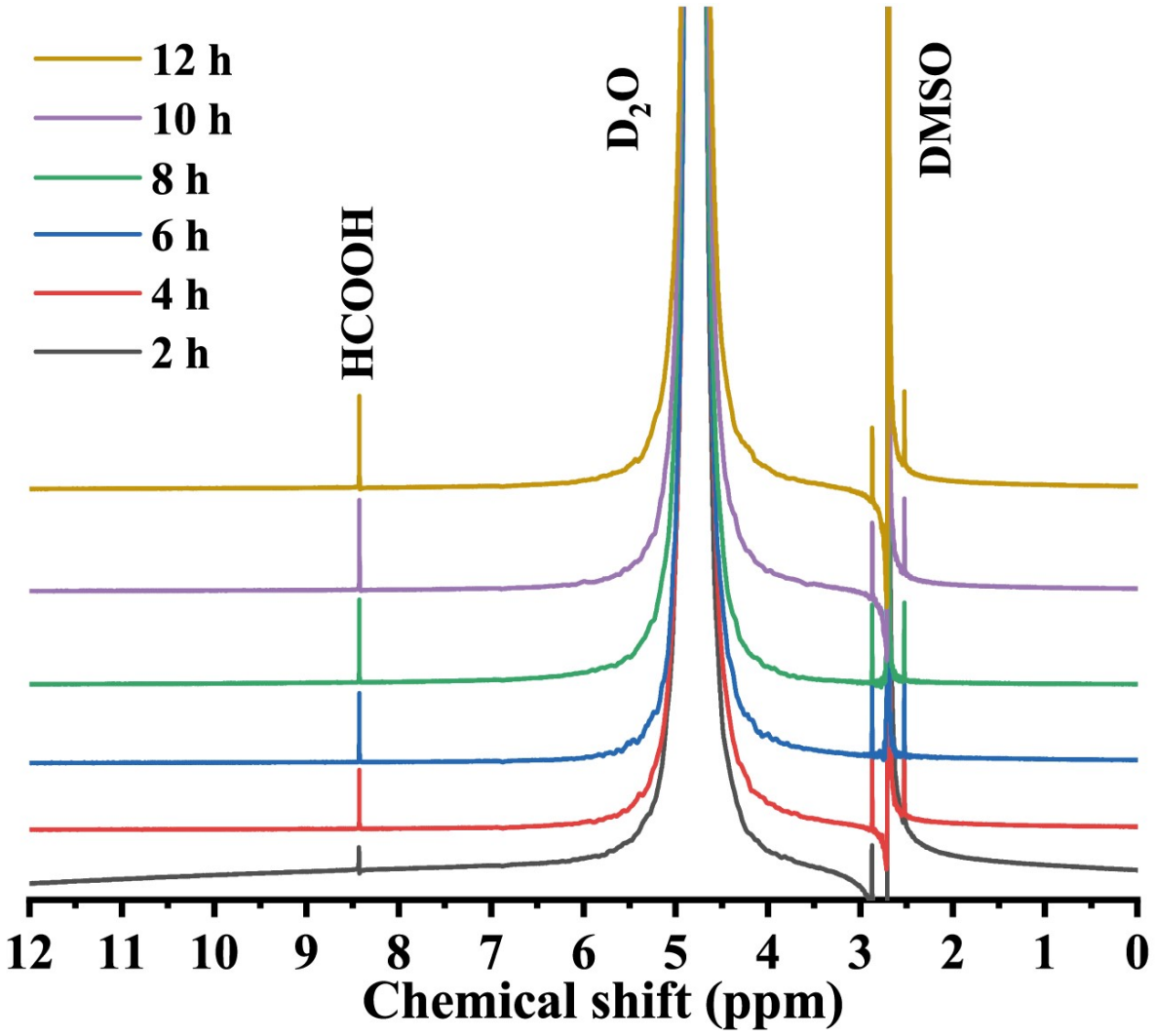

Figure S9. ^{1}H NMR spectra of the CO_2RR liquid products of $Cu_{96}Al_4$ nanocrystal tested at −0.8 V vs. RHE for 12 h. The liquid sample was obtained at 2 h intervals.

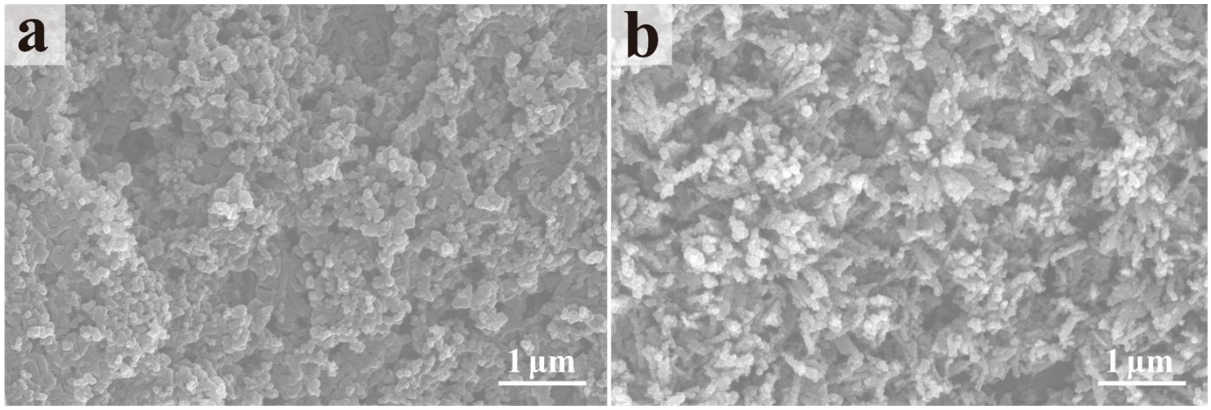

Figure S10. SEM images of $Cu_{96}Al_4$ nanocrystal (a) before and (b) after 12 hours of CO_2RR at −0.8 V vs. RHE.

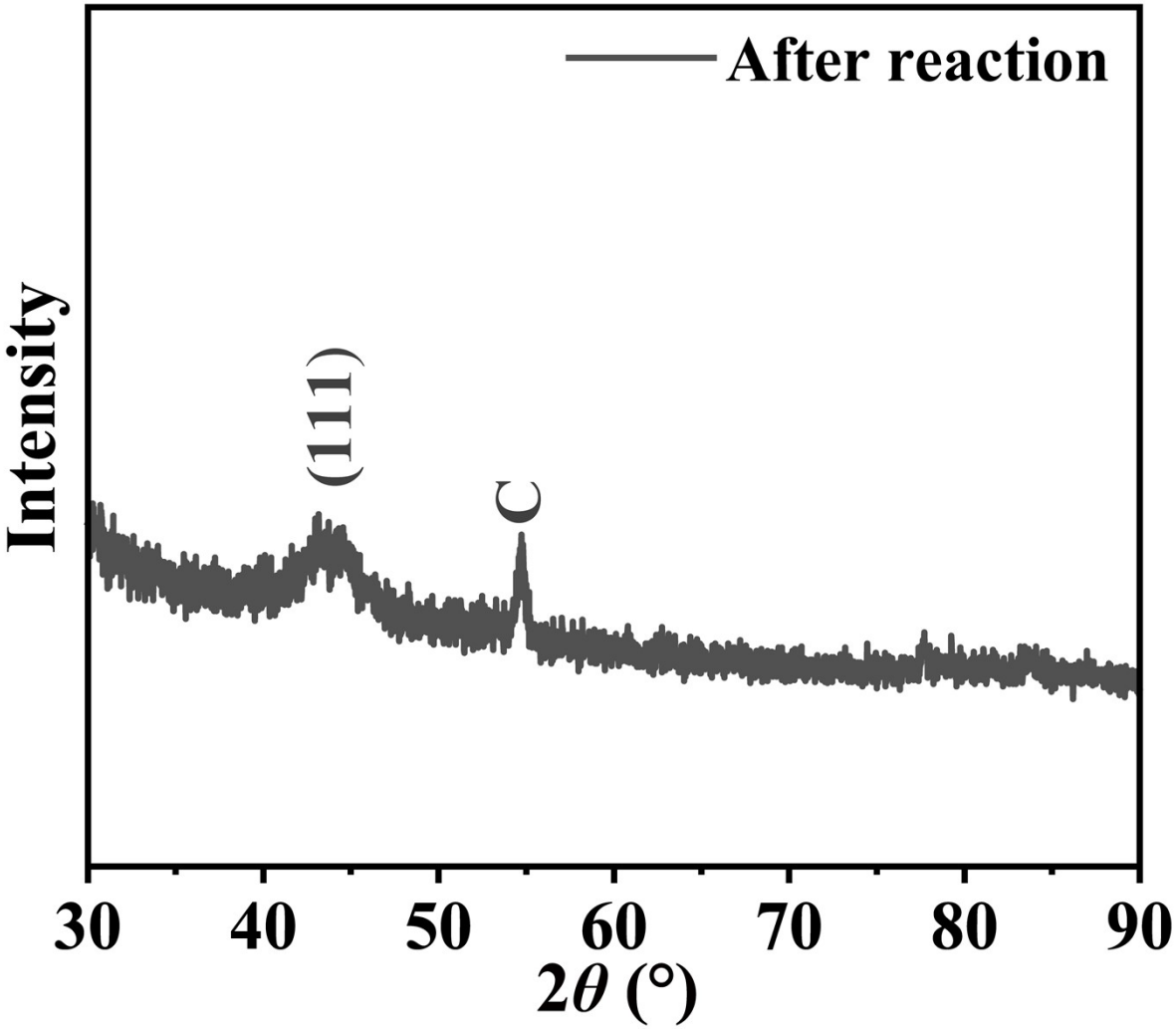

Figure S11. XRD pattern of $Cu_{96}Al_4$ nanocrystal after 12 h of CO_2RR at −0.8 V vs. RHE.

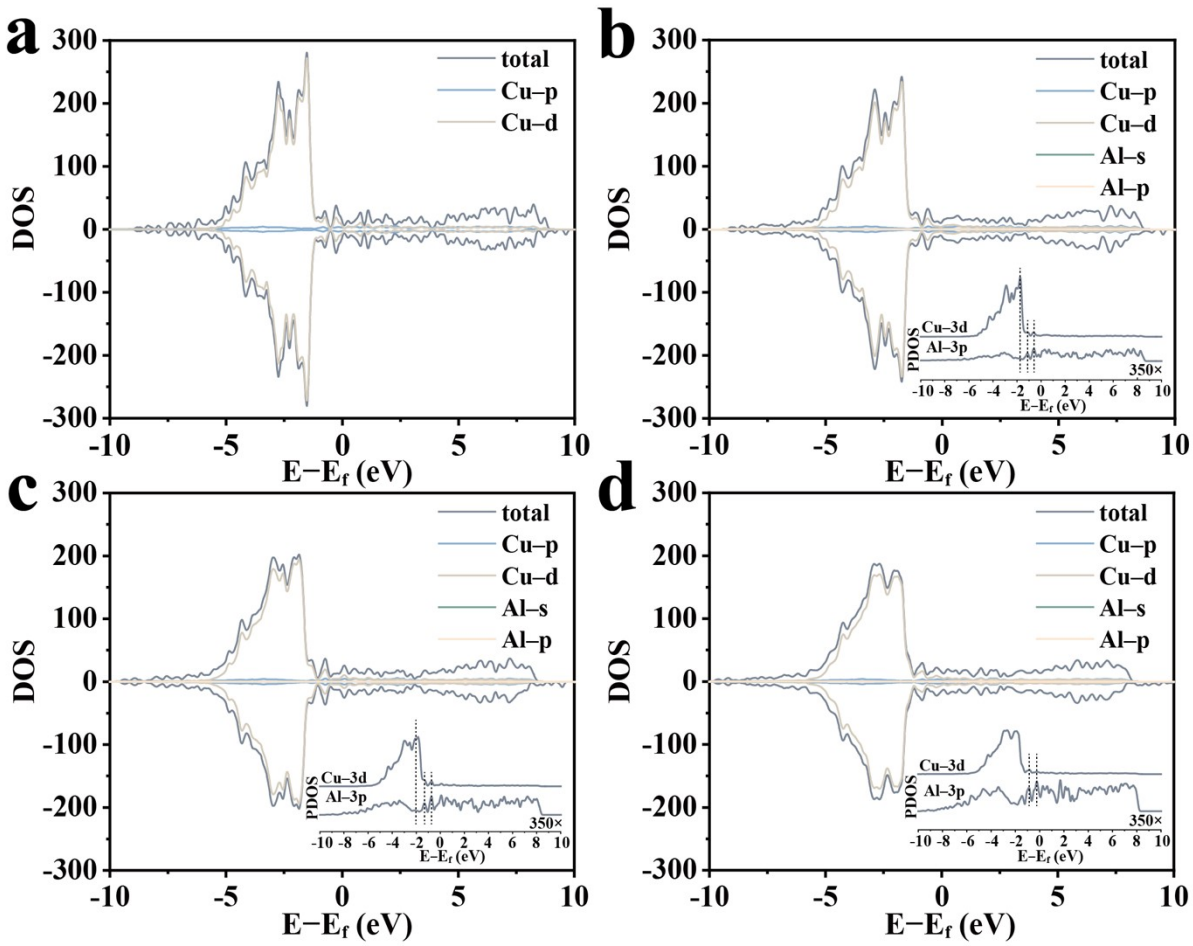

Figure S12. The total density of states (DOS) of (a) Cu, (b) $Cu_{96}Al_4$, (c) $Cu_{93}Al_7$, and (d) $Cu_{88}Al_{12}$ nanocrystals. The insets are projected DOS (PDOS) of Cu–3d and Al–3p orbitals magnified 350×.

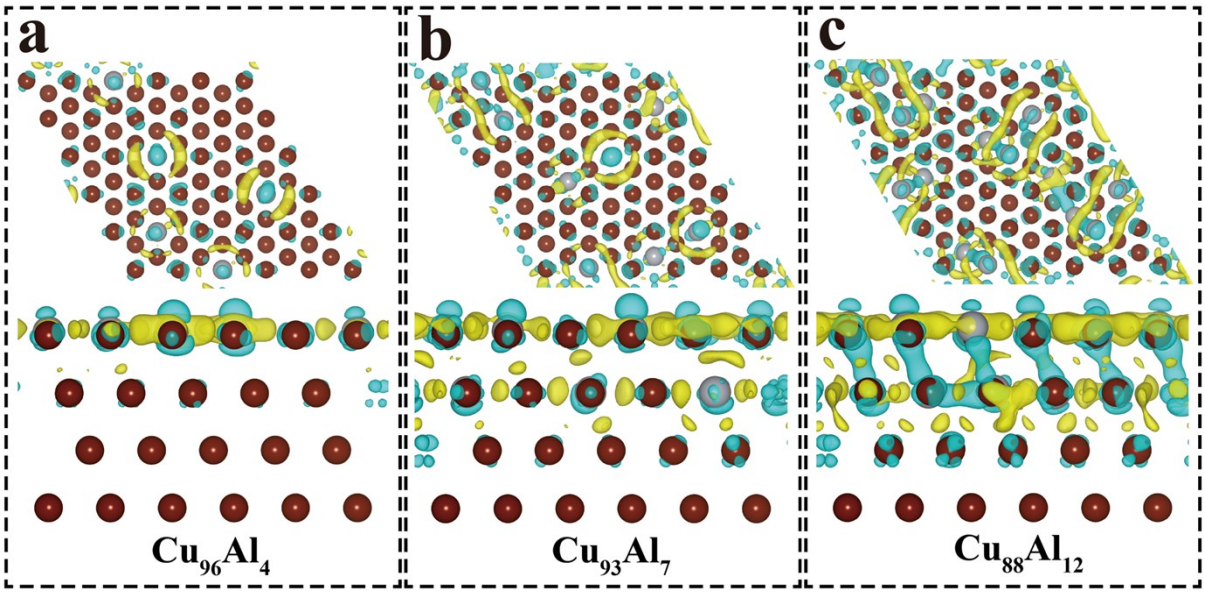

Figure S13. Schematic illustration of the Bader charge of (a) $Cu_{96}Al_4$, (b) $Cu_{93}Al_7$, and (c) $Cu_{88}Al_{12}$ nanocrystals. The above is a top view, and the below is a side view. Yellow and cyan regions represent electron accumulation and depletion, separately.

Table S1. The elemental analyses of Cu, $Cu_{96}Al_4$, $Cu_{93}Al_7$, and $Cu_{88}Al_{12}$ single crystals using HAADF-STEM EDS.

Samples	**Cu (at%)**	**Al (at%)**
Cu	97.78	
$Cu_{96}Al_4$	96.27	3.73
$Cu_{93}Al_7$	92.79	7.21
$Cu_{88}Al_{12}$	87.66	12.34

Table S2. The values of the equivalent circuit element in the EIS diagrams of Cu, $Cu_{96}Al_4$, $Cu_{93}Al_7$, and $Cu_{88}Al_{12}$ nanocrystals. The R_s, R_{ct}, and R_{total} represent the solution resistance, charge transfer resistance, and the total resistance, respectively.

Samples	R_s **(Ω)**	R_{ct} **(Ω)**	R_{total} **(Ω)**
Cu	7.77	3.12	10.89
$Cu_{96}Al_4$	7.4	1.34	8.74
$Cu_{93}Al_7$	8.23	3.98	12.21
$Cu_{88}Al_{12}$	8.76	5.91	14.67

Table S3. The comparison of FE for Cu-based alloy catalysts in H-type cells.

Catalysts	Electrolytes	Potential (vs. RHE)	Products	FE (%)	Refs.
$Cu_{96}Al_4$	0.5 M $KHCO_3$	−0.8 V	HCOOH, CO	**77.71, 18.01**	This work
Cu				76.43, 13.32	
$Cu_{93}Al_7$				72.24, 12.91	
$Cu_{88}Al_{12}$				67.51, 7.66	
Cu−SnO_2	0.5 M $KHCO_3$	−0.9 V	HCOOH	92	1
O_p−Ag_1In	0.5 M $NaHCO_3$	−0.95 V	HCOOH	92.03	2
$Ga_{83.2}In_{16.8}$	0.1 M $KHCO_3$	−1.9 V	HCOOH	98	3
$Sb_{25}Bi_{75}$	0.5 M $KHCO_3$	−1.0 V	HCOOH	~85	4
CuPd-1.5-alloy	0.5 M $KHCO_3$	−0.7 V	CH_3COOH, C_{1+}	46.5±2.1, ~37	5
$PdCu_3$/NC	0.1 M $KHCO_3$	−0.5 V	CO	99.8	6
Cu_5Ga_1	0.1 M $KHCO_3$	−1.0 V	C_{1+}, C_{2+}	~85	7
Cu-Zn	0.1 M $KHCO_3$	−1.0 V	EtOH, C_{2+}	19, 56	8
$Tb_{2.9}$PAT	0.5 M $KHCO_3$	−0.8 V	CO	95.7	9
V-$CuInSe_2$	0.5 M $KHCO_3$	−0.7 V	CO	91	10
Ag_{65}−Cu_{35} JNS 100	0.1 M $KHCO_3$	−1.4 V	C_{1+}, C_{2+}	15, 72.1	11
BiCu-SAA	0.1 M $KHCO_3$	−1.1 V	C_{1+}, C_{2+}	~14, 73.4	12
$CuGa_{17}$	0.1 M $KHCO_3$	−1.2 V	C_{1+}, C_{2+}	~75	13
$Bi_{85}Pb_{15}$	0.2 M $KHCO_3$	−1.0 V	HCOOH	96.5	14
CuSn NPs/C−H	0.1 M $KHCO_3$	−1.0 V	CO, HCOOH	~90	15
$Cu_{0.07}Zn$	0.1 M $KHCO_3$	−1.15 V	CO	77.3	16
Pd@Pd_3Au_7	0.1 M $KHCO_3$	−0.5 V	CO	94	17
CuSn-4	0.5 M $KHCO_3$	−1.4 V	HCOOH	87.7	18
Pd_4Ag	0.1 M $KHCO_3$	−0.23 V	HCOOH	94	19
BiPdC	0.1 M $KHCO_3$	−0.97 V	HCOOH	63.41	20
AuCu/Cu-SCA	0.5 M $KHCO_3$	−1.0 V	C_{1+}, C_{2+}	~78	21
Cu-Pd	0.1 M $KHCO_3$	−0.9 V	CO	87	22
Cu_3−Ag_3Au	0.1 M $KHCO_3$	−1.2 V	C_2H_4, C_{1+}	69±5, ~20	23
CuIn-1 mM	0.1 M $KHCO_3$	−1.0 V	CO	86	24
s-PdNi/CNFs-1000	0.1 M $KHCO_3$	−0.88 V	CO	96.6	25
Cu−Ag	0.1 M $KHCO_3$	−1.0 V	C_{1+}, C_{2+}	~90	26
AuAg-R	0.1 M $KHCO_3$	−0.87V	CO	>80	27
Cu−In_2O_3/C	0.1 M $KHCO_3$	−0.7 V	CO	95	28
Ag@Cu_2O	0.1 M $KHCO_3$	−1.6 V	C_{1+}, C_{2+}	~10, 78.5	29
$Cu_{70}Zn_{30}$ NPs	0.1 M $KHCO_3$	−1.35 V	C_{1+}, C_{2+}	~80.2	30
S-CuSn	0.5 M $KHCO_3$	−1.2 V	HCOOH	91.5	31
PdIn@In_2O_3	0.5 M $KHCO_3$	−0.9 V	CO	75.36	32
4H/fcc Au@Cu	0.1 M $KHCO_3$	−0.82 V	C_{1+}, C_{2+}	~91	33
$Au_{50}Ag_{50}$	0.1 M $KHCO_3$	−0.7 V	CO	97.8	34
Cu_1Fe_2/NC	0.5 M $KHCO_3$	−0.7 V	CO	98.91	35

Table S4. FE of the CO_2RR for $Cu_{96}Al_4$ nanocrystal tested at −0.8 V vs. RHE for 12 h. The gas and liquid products were recorded at 2 h intervals.

Time (h)	FE_{HCOOH} (%)	FE_{CO} (%)	FE_{H_2} (%)	FE_{C1} (%)
2	77.61	16.91	4.88	94.52
4	78.38	15.92	4.74	94.3
6	75.98	16.66	6.25	92.64
8	74.4	16.47	6.16	90.87
10	70.43	16.73	7.88	87.16
12	46.04	9.35	42.85	55.39

References

1 B. Li, J. Chen, L. Wang, D. Xia, S. Mao, L. Xi, S. Ying, H. Zhang and Y. Wang, *Appl. Catal. B: Environ.*, 2025, **363**, 124784.

2 C. Fang, L. Huang, W. Gao, X. Jiang, H. Liu, R. Hu, X. Li, J. Yu and W. Zhou, *Adv. Energy Mater.*, 2024, **14**, 2400813.

3 F. Gholampoursaadi, X. Zhi, S. Nour, J. Z. Liu, G. K. Li and M. Mayyas, *Adv. Funct. Mater.*, 2024, **34**, 2316435.

4 J. Sun, W. Yang, B. Yu, Y. Liu, Y. Zhao, G. Cheng and Z. Zhang, *J. Mater. Chem. A*, 2025, **13**, 5661–5669.

5 S. Nie, L. Wu, Q. Liu and X. Wang, *J. Am. Chem. Soc.*, 2024, **146**, 29364–29372.

6 J. Dong, Y. Cheng, Y. Li, X. Peng, R. Zhang, H. T. Wang, C. Wang, X. Li, P. Ou, C. W. Pao, L. Han, W. F. Pong, Z. Lin, J. Luo and H. L. Xin, *ACS Appl. Mater. Interfaces*, 2022, **14**, 41969–41977.

7 L. Chen, J. Chen, W. Fu, J. Chen, D. Wang, Y. Xiao, S. Xi, Y. Ji and L. Wang, *Nat. Commun.*, 2024, **15**, 7053.

8 A. Herzog, M. Rüscher, H. S. Jeon, J. Timoshenko, C. Rettenmaier, U. Hejral, E. M. Davis, F. T. Haase, D. Kordus, S. Kühl, W. Frandsen, A. Bergmann and B. Roldan Cuenya, *Energy Environ. Sci.*, 2024, **17**, 7081–7096.

9 Y. Xu, Y. Wang, P. Wang, Y. Wang, W. Dai, J. Zou and X. Luo, *J. Colloid Interf. Sci.*, 2024, **673**, 346–353.

10 J. Wang, X. Zheng, G. Wang, Y. Cao, W. Ding, J. Zhang, H. Wu, J. Ding, H. Hu, X. Han, T. Ma, Y. Deng and W. Hu, *Adv. Mater.*, 2021, **34**, 2106354.

11 Y. Ma, J. Yu, M. Sun, B. Chen, X. Zhou, C. Ye, Z. Guan, W. Guo, G. Wang, S. Lu, D. Xia, Y. Wang, Z. He, L. Zheng, Q. Yun, L. Wang, J. Zhou, P. Lu, J. Yin, Y. Zhao, Z. Luo, L. Zhai, L. Liao, Z. Zhu, R. Ye, Y. Chen, Y. Lu, S. Xi, B. Huang, C. S. Lee and Z. Fan, *Adv. Mater.*, 2022, **34**, 2110607.

12 Y. Cao, S. Chen, S. Bo, W. Fan, J. Li, C. Jia, Z. Zhou, Q. Liu, L. Zheng and F. Zhang, *Angew. Chem. Int. Ed.*, 2023, **135**, e202303048.

13 V. Okatenko, A. Loiudice, M. A. Newton, D. C. Stoian, A. Blokhina, A. N. Chen, K. Rossi and R. Buonsanti, *J. Am. Chem. Soc.*, 2023, **145**, 5370–5383.

14 S. Farid, A. Rashid, K. S. Joya and F. Yasmeen, *J. Mater. Chem. A*, 2025, **13**, 14010–14023.

15 P. Wang, M. Qiao, Q. Shao, Y. Pi, X. Zhu, Y. Li and X. Huang, *Nat. Commun.*, 2018, **9**, 4933.

16 R. Zou, R. Luo, F. Liu, Y. Wang, M. S. Riaz, S. Shen, G. Yang, Z. Tang, H. Huang, G. Li and Q. Bi, *Small*, 2025, DOI: 10.1002/smll.202501030, 2501030.

17 X. Yuan, L. Zhang, L. Li, H. Dong, S. Chen, W. Zhu, C. Hu, W. Deng, Z. J. Zhao and J. Gong, *J. Am. Chem. Soc.*, 2019, **141**, 4791–4794.

18 Y. Li, C. Z. Huo, H. J. Wang, Z. X. Ye, P. P. Luo, X. X. Cao and T. B. Lu, *Nano Energy*, 2022, **98**, 107277.

19 N. Han, M. Sun, Y. Zhou, J. Xu, C. Cheng, R. Zhou, L. Zhang, J. Luo, B. Huang and Y. Li, *Adv. Mater.*, 2020, **33**, 2005821.

20 S. Gao, S. Chen, Q. Liu, S. Zhang, G. Qi, J. Luo and X. Liu, *ACS Appl. Nano Mater.*,

2022, **5**, 12387–12394.
21 S. Shen, X. Peng, L. Song, Y. Qiu, C. Li, L. Zhuo, J. He, J. Ren, X. Liu and J. Luo, *Small*, 2019, **15**, 1902229.
22 Y. Mun, S. Lee, A. Cho, S. Kim, J. W. Han and J. Lee, *Appl. Catal. B: Environ.*, 2019, **246**, 82–88.
23 L. Xiong, X. Zhang, H. Yuan, J. Wang, X. Yuan, Y. Lian, H. Jin, H. Sun, Z. Deng, D. Wang, J. Hu, H. Hu, J. Choi, J. Li, Y. Chen, J. Zhong, J. Guo, M. H. Rümmerli, L. Xu and Y. Peng, *Angew. Chem. Int. Ed.*, 2020, **60**, 2508–2518.
24 Q. Zhou, X. Tang, S. Qiu, L. Wang, L. Hao and Y. Yu, *Mater. Today Phys.*, 2023, **33**, 101050.
25 J. Hao, Z. Zhuang, J. Hao, K. Cao, Y. Hu, W. Wu, S. Lu, C. Wang, N. Zhang, D. Wang, M. Du and H. Zhu, *ACS Nano*, 2022, **16**, 3251–3263.
26 Y. Qiao, G. Kastlunger, R. C. Davis, C. A. G. Rodriguez, A. Vishart, W. Deng, Q. Xu, S. Li, P. Benedek, J. Chen, J. Schröder, J. Perryman, D. U. Lee, T. F. Jaramillo, I. Chorkendorff and B. Seger, *ACS Catal.*, 2023, **13**, 9379–9391.
27 H. Yun, W. Choi, D. Shin, H. S. Oh and Y. J. Hwang, *ACS Catal.*, 2023, **13**, 9302–9312.
28 Y. Jia, H. S. Hsu, W. C. Huang, D. W. Lee, S. W. Lee, T. Y. Chen, L. Zhou, J. H. Wang, K. W. Wang and S. Dai, *Nano Lett.*, 2023, **23**, 2262–2268.
29 Y. Lu, H. Li, H. Sun, J. Zhao, Y. Zhang, Y. Wang, C. Zhu, D. Gao, Y. Tuo, J. Zeng, D. Chen and Z. Yan, *ACS Catal.*, 2024, **14**, 14744–14753.
30 H. S. Jeon, J. Timoshenko, F. Scholten, I. Sinev, A. Herzog, F. T. Haase and B. Roldan Cuenya, *J. Am. Chem. Soc.*, 2019, **141**, 19879–19887.
31 K. Li, J. Xu, T. Zheng, Y. Yuan, S. Liu, C. Shen, T. Jiang, J. Sun, Z. Liu, Y. Xu, M. Chuai, C. Xia and W. Chen, *ACS Catal.*, 2022, **12**, 9922–9932.
32 D. Bagchi, S. Sarkar, A. K. Singh, C. P. Vinod and S. C. Peter, *ACS Nano*, 2022, **16**, 6185–6196.
33 Y. Chen, Z. Fan, J. Wang, C. Ling, W. Niu, Z. Huang, G. Liu, B. Chen, Z. Lai, X. Liu, B. Li, Y. Zong, L. Gu, J. Wang, X. Wang and H. Zhang, *J. Am. Chem. Soc.*, 2020, **142**, 12760–12766.
34 J. Mo, D. Lou, J. Li, X. Tao, Z. Zheng and W. Liu, *J. Colloid Interf. Sci.*, 2025, **697**, 137934.
35 Y. Song, Y. Hua, X. Liu and Z. Gao, *J. Alloys Compd.*, 2025, **1022**, 179927.